Available online at www.sciencedirect.com

ScienceDirect

IFAC Papers Online CONFERENCE PAPER ARCHIVE

IFAC-PapersOnLine 48-16 (2015) 235–240

Supervisory Control of Line Breakage for Thruster-Assisted Position Mooring System

Zhengru Ren * **Roger Skjetne** * **Vahid Hassani** * [1]

* *Department of Marine Technology, Norwegian University of Science and Technology, NO 7491 Trondheim, Norway, (e-mail: zhengrur@stud.ntnu.no, {roger.skjetne, vahid.hassani}@ntnu.no)*

Abstract: Thruster-assisted position mooring (TAPM) is an energy-efficient and reliable stationkeeping method for deep water structures. Mooring line breakage can significantly influence the control system, and ultimately reduce the reliability and safety during operation and production. Therefore, line break detection is a crucial issue for TAPM systems. Tension measurement units are useful tools to detect line failures. However, these units increase the building cost of the system, and in a large portion of existing units in operation line tension sensors are not installed. This paper presents a fault-tolerant control scheme based on estimator-based supervisory control methodology to detect and isolate a line failure with only position measurements. After detecting a line break, a supervisor switches automatically a new controller into the feedback loop to keep the vessel within the safety region. Numerical simulations are conducted to verify the performance of the proposed technique, for a turret-based mooring system.

Keywords: Thruster-Assisted Position Mooring; Supervisory Control; TAPM; Mooring Line Breakage; Fault Diagnosis

1 Introduction

With the depletion of onshore oil and gas resources, energy companies have brought about increasing interest in the exploration and exploitation of offshore and deeper resources. Dynamic positioning (DP) systems are used in offshore drilling applications to ensure stationkeeping of the drilling vessel. A thruster-assisted position mooring (TAPM) system is another solution in which the mooring system decreases the level of thrust needed. This allows the thrusters to improve the positionkeeping performance. For a DP system, both the position and heading should be kept at the desired values by the thrusters only. In a normal sea, a TAPM system will keep the vessel in a reasonable region by the mooring lines, while the thrusters support the system in keeping the optimal heading and additional surge-sway damping.

Early DP systems were implemented using PID controllers with notch filters in cascade with lowpass filters. Later, more advanced model-based control techniques, such as linear quadratic Gaussian controllers were applied; see Balchen et al. (1976, 1980). Robust H_∞ DP controller (Hassani et al., 2012a,b) and nonlinear controllers such as backstepping (see Fossen and Grøvlen (1998)) and sliding-mode control (Tannuri et al., 2001) are reported. Using a mooring model in the design of a mooring-assisted DP system is proposed by Aamo and Fossen (1999), where the tension of each mooring line is controlled using a finite element method (FEM) model. Chen et al. (2013) applied a neural network approximation and used the backstepping technique to control the mooring system. Structural reliability and fault-tolerant control are applied to control the position mooring (Berntsen et al., 2006, 2009; Fang et al., 2013). Application of fault monitoring and fault recovery control techniques to position-moored vessels are proposed and tested (Fang and Blanke, 2011; Fang et al., 2015).

Mooring line failures can lead to a loss of positionkeeping capability in the floating structure. Hence, it can endanger human lives, equipments, and the environment. Mooring line failures can happen at both the upper and bottom ends, and they may not be found within several months. A series of guidance documents and standards about position mooring system are published from the main associations and class societies, such as API (2005), ABS (2014), and DNV (2010). All these guidelines and standards require a redundancy to line break during the mooring design stage. Many industrial products have been invented to provide real-time monitoring of the mooring and riser systems. Pulse Structural Monitoring developed the world's first low cost motion logger, the INTEGRIpod™, in 1998 (Gauthier et al., 2014). With integrated data loggers for measuring the movement of subsea structures, the system will alert when the tension in a mooring line exceeds the preset threshold. Similarly, Inter-M Pulse™ is suitable for moored FPSO and mobile offshore drilling units (MODU) to provide full history data with acoustic signals (Elman et al., 2013). However, according to statistical data, 50% of the floating production storage and offloadings (FPSOs) in the North Sea cannot monitor line tension in real time, and 78% of them do not have line failure alarms (Brown et al., 2005).

This paper presents a fault-tolerant control scheme based on an estimator-based supervisory control method to detect line failures with only position measurements. It can detect line break without tension measurements, and thereafter switch automatically to a fault handling control mode to safely position the vessel. This method can thus improve the system's redundancy and safety with only a software update.

[1] Vahid Hassani is also a researcher at the Norwegian Marine Technology Research Institute (MARINTEK).

10.1016/j.ifacol.2015.10.286

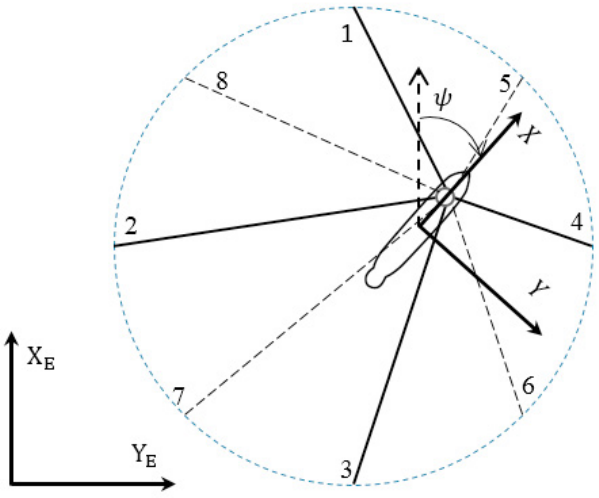

Fig. 1. Reference frames and the spread mooring system.

2 System Modeling

Stationkeeping by a TAPM system is achieved using a combination of DP and turret-based mooring with M anchor lines. In this case study, $M = 8$. It is assumed that the mooring system is symmetrically arranged. All possible configurations of the mooring system, including fault-free and faulty modes, are listed in Table 1, where $p \in \boldsymbol{\mathcal{P}}$ where $\boldsymbol{\mathcal{P}} = \{0, 1, 2, \cdots, M\}$ is an index set which corresponds with one fault-free mode and M faulty modes.

Table 1. Events for the index.

Modes P_p	Description	Observer	Controller
P_0(normal)	No line breaks	Observer 0	Controller 0
P_1, P_2, P_3, P_4	Line 1/2/3/4	Observer	Controller
P_5, P_6, P_7, P_8	5/6/7/8 breaks	1/2/3/4	1/2/3/4
(faulty)		5/6/7/8	5/6/7/8

2.1 Floating vessel dynamics

In what follows, the low frequency control plant model $\mathbb{P}$ is given by

$$\dot{\boldsymbol{\eta}} = \boldsymbol{R}(\boldsymbol{\psi})\boldsymbol{\nu}, \tag{1a}$$

$$\boldsymbol{M}\dot{\boldsymbol{\nu}} + \boldsymbol{D}\boldsymbol{\nu} = \boldsymbol{R}(\psi)^{\top}\boldsymbol{b} + \boldsymbol{\tau_m} + \boldsymbol{\tau_c}, \tag{1b}$$

$$\dot{\boldsymbol{b}} = \boldsymbol{0}, \tag{1c}$$

where $\boldsymbol{\eta}$ consists of low frequency (LF) Earth-fixed position and LF heading orientation of the vessel relative to an Earth-fixed frame, $\boldsymbol{\nu}$ represents linear and rotational velocities decomposed in a vessel-fixed reference, and $\boldsymbol{R}(\psi) \in \mathbb{R}^{3\times3}$ denotes the transformation matrix between the body-fixed frame and Earth-fixed frame (Fossen, 2011). Fig. 1 presents the reference frames.

Equation (1b) describes the vessel's LF motion at low speed, $\boldsymbol{M} \in \mathbb{R}^{3\times3}$ is the generalized system inertia matrix including zero frequency added mass components, $\boldsymbol{D}$ denotes the linear damping matrix, $\boldsymbol{\tau_m}$, $\boldsymbol{\tau_c}$ and $\boldsymbol{b} \in \mathbb{R}^3$ are the mooring loads, and thruster-induced forces/moments, and the slow varying bias vector in the earth frame, respectively.

2.2 Mooring forces

The mooring system is typically described by catenary equations, disregarding the cable dynamics, the higher mode full-profile motion, nonlinear damping, and vibrations. For the LF motion model, a horizontal-plane spread mooring model is formulated as

$$\boldsymbol{\tau_m} = -\boldsymbol{R}^{\top}(\psi)\boldsymbol{g}_{mo}(\boldsymbol{\eta}) - \boldsymbol{d}_{mo}(\boldsymbol{\nu}). \tag{2}$$

Assuming fixed mooring line length, damping effects of mooring line $\boldsymbol{d_{mo}}(\boldsymbol{\nu}) \in \mathbb{R}^3$ can be approximated by a linearized mooring damping matrix $\boldsymbol{D_{mo}\nu}$. It is a common practice to estimate the linear damping of the mooring line by about $10-20\%$ of critical damping of the entire system (Nguyen et al., 2011). We have augmented the estimated linear damping of the mooring system into the damping term $\boldsymbol{D\nu}$ in the left hand side of (1b). The Earth-fixed restoring force component $\boldsymbol{g_{mo}}(\boldsymbol{\eta}) \in \mathbb{R}^3$ is given by

$$\boldsymbol{g}_{mo} = \boldsymbol{T}(\boldsymbol{\beta})\boldsymbol{L}_p\boldsymbol{\tau}_H, \tag{3}$$

where $\boldsymbol{\tau}_H \in \mathbb{R}^M$ is the horizontal component of the tension, and $\boldsymbol{L}_p \in \mathbb{R}^{M\times M}$ is a diagonal coefficient matrix denoting the line breakage information. Under the fault-free conditions, $\boldsymbol{L}_0 = \boldsymbol{I}$. When the p^{th} mooring line breaks (P_p), the p^{th} diagonal element of $\boldsymbol{L}_p$ is 0 while the other diagonal elements are 1. The turret can rotate around the center of turret (COT). The mooring line configuration matrix $\boldsymbol{T}(\boldsymbol{\beta}) \in \mathbb{R}^{3\times M}$ is given by

$$\boldsymbol{T}(\boldsymbol{\beta}) = \begin{bmatrix} cos\beta_1 & \cdots & cos\beta_M \\ sin\beta_1 & \cdots & sin\beta_M \\ \bar{x}_1 sin\beta_1 - \bar{y}_1 cos\beta_1 & \cdots & \bar{x}_N sin\beta_N - \bar{y}_N cos\beta_N \end{bmatrix}, \tag{4}$$

where $\boldsymbol{\beta} = [\beta_1, \cdots, \beta_M] \in \mathbb{R}^M$ is the mooring line orientation vector consisting of the angles between the mooring lines and the x-axis, $\bar{x}_i \in \bar{\boldsymbol{x}}$ and $\bar{y}_i \in \bar{\boldsymbol{y}}$ are the horizontal displacements of the i^{th} $(i = 1\cdots M)$ mooring line between turret terminal point (TP) and Anchor i cable. The horizontal mooring force vector is denoted by $\boldsymbol{\tau}_H = [H_1, H_2, \cdots, H_M]^{\top}$, where H_i represents the horizontal force component at TP_i. Fig. 2 shows the configuration of a single mooring line. It is assumed that the yaw moment acting on the vessel through the turret is zero. The 2D catenary equations (5a) and (5b) are used in this case to calculate H_i and the vertical mooring force component V_i (Aamo and Fossen, 2001).

$$x_i(s) = \frac{H_i}{E_m A_m}s + \frac{H_i}{\omega_m}\left\{ sinh^{-1}\left[\frac{V_i - \omega_m(L_m - s)}{H_i}\right] - sinh^{-1}\left[\frac{V_i - \omega_m L_m}{H_i}\right]\right\}, \tag{5a}$$

$$z_i(s) = \frac{1}{E_m A_m}\left[V_i s + \frac{\omega_m}{2}\left((L_m - s)^2 - L_m^2\right)\right] + \frac{H_i}{\omega_m}\left[\sqrt{1 + \left(\frac{V_i - \omega_m(L_m - s)}{H_i}\right)^2} + \sqrt{1 + \left(\frac{V_i - \omega_m L_m}{H_i}\right)^2}\right], \tag{5b}$$

where $x_i(s)$ and $z_i(s)$ are the positions of each segment centered at length s along the i^{th} cable, ω_m is the weight in water per unit length, E_m is the Young's modulus of elasticity, A_m stands for the cross-section area of the line, and $T_i = \sqrt{V_i^2 + H_i^2}$ is tension at the end of the i^{th} mooring line, $0 \le s \le L_m$ is the path parameter along the cable, and L_m and L_d are the suspended segment length and the touchdown length respectively. The mooring line can be categorized into the touchdown and the suspended catenary. When the attachment point moves in either the horizontal plane or the vertical plane, L_m and L_d vary. $L = L_d + L_m$ denotes the unstretched length of the mooring lines.

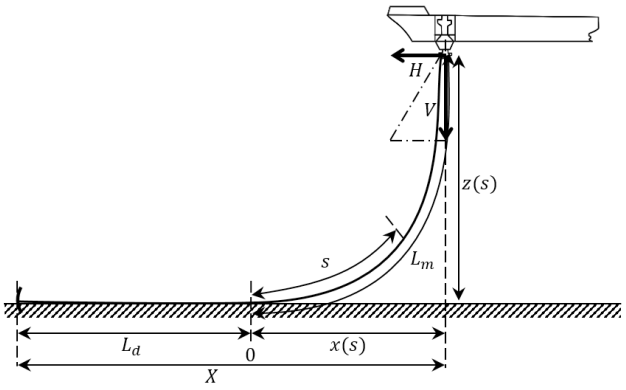

Fig. 2. Mooring line configuration.

3 Supervisory Control

In this case, we have M known single-fault scenarios, single-line failures, as well as their known faulty models. Thus, this paper is based on a hypothesis that the broken line no longer provides horizontal restoring force. Hence, all faulty models and events are known.

Quantitative model-based methods can be divided into three main categories: state estimation, parameter estimation, and parity space method (Stoican and Olaru, 2013). In this paper, a state estimation method is employed. In supervisory control, the controllers are pre-designed, and the fault diagnosis is conducted by online monitoring. The supervisory controller consists of a bank of candidate controllers designed such that each of them can control the system during a specific line failure mode. A supervisor uses real-time input and output data, and prior information about the system, to generate a switching signal that determines which controller to use at what time. In this methodology, a separate controller that provides satisfactory performance for all the possible mooring line failures, should be designed and included in the bank of controllers.

For each failure mode in the mooring line system, an individual observer is designed. The resulting set of observers forms a bank which runs in parallel. At each sampling instant a nonlinear function of the measurement residuals are used to compute a performance signal for each observer. The rationale is that the most accurate estimator will have the best performance signal. In each sample time, the performance signals are assessed to decide which controller to select. Fig. 3 shows the architecture of the multi-estimator based supervisory control. This is built upon a well-known heuristic idea of certainty equivalence, where the principle of the switching logic is to find the observer with closest output to the process output (Hespanha, 2001).

3.1 Observer design

Passive observers were introduced in the late 1990s (Fossen and Strand, 1999; Hassani and Pascoal, 2015). The main motivation is to avoid tuning a large number of parameters in designing a Kalman filter. The nonlinear passive observer $\mathbb{E}$ corresponding to the p^{th} operation mode admits the realization

$$\dot{\hat{\boldsymbol{\eta}}}_{w,p} = \boldsymbol{A_{pw}}(\omega_0)\hat{\boldsymbol{\eta}}_{w,p} + \boldsymbol{K_1}\tilde{\boldsymbol{y}}_p, \tag{6a}$$

$$\dot{\hat{\boldsymbol{\eta}}}_p = \boldsymbol{R}(\psi)\hat{\boldsymbol{\nu}}_p + \boldsymbol{K_2}\tilde{\boldsymbol{y}}_p, \tag{6b}$$

$$\dot{\hat{\boldsymbol{b}}}_p = -\boldsymbol{T_b^{-1}}\hat{\boldsymbol{b}}_p + \boldsymbol{K_3}\tilde{\boldsymbol{y}}_p, \tag{6c}$$

$$\begin{aligned}\boldsymbol{M}\dot{\hat{\boldsymbol{\nu}}}_p = &- \boldsymbol{D}\hat{\boldsymbol{\nu}}_p + \boldsymbol{R}(\psi)^\top\hat{\boldsymbol{b}}_p - \boldsymbol{R}(\psi)^\top\boldsymbol{T}(\hat{\boldsymbol{\beta}})\boldsymbol{L}_p\hat{\boldsymbol{\tau}}_H \\ &+ \boldsymbol{\tau}_c + \boldsymbol{K_4}\boldsymbol{R}(\psi)^\top\tilde{\boldsymbol{y}}_p,\end{aligned} \tag{6d}$$

$$\hat{\boldsymbol{y}}_p = \hat{\boldsymbol{\eta}}_p + \boldsymbol{C}_{pw}\hat{\boldsymbol{\eta}}_{w,p}, \quad p \in \boldsymbol{\mathcal{P}}, \tag{6e}$$

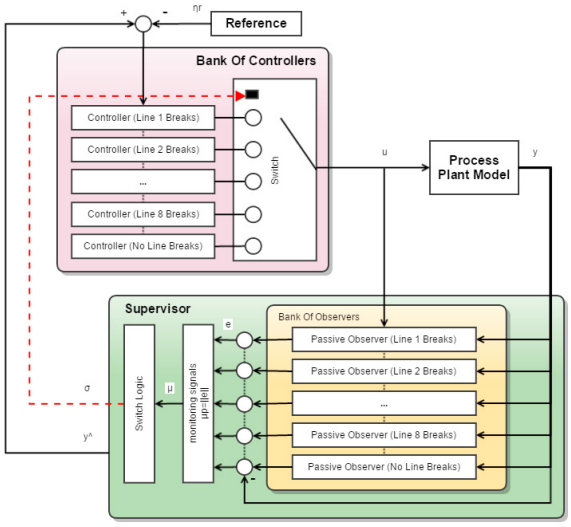

Fig. 3. Supervisory control for a TAPM system, adjusted from Nguyen et al. (2007).

where $\boldsymbol{A_{pw}}$ and $\boldsymbol{C_{pw}}$ are the system matrix and measurement matrix of the linear filter which models the wave-induced motions of the vessel as a result of first order wave effects. $\tilde{\boldsymbol{y}}_p = \boldsymbol{y} - \hat{\boldsymbol{y}}_p$ is the output estimation error, $\hat{\boldsymbol{\eta}}_w$ is the estimated wave-induced motion vector, $\boldsymbol{L}_p$ is the only matrix that varies in the bank of the observers, and $\hat{\boldsymbol{\tau}}_H$ is estimated by the projected horizontal distance between the anchor and TP, see (7). $\boldsymbol{K_1} \in \mathbb{R}^{6\times3}$, $\boldsymbol{K_2} \in \mathbb{R}^{3\times3}$, $\boldsymbol{K_3} \in \mathbb{R}^{3\times3}$, and $\boldsymbol{K_4} \in \mathbb{R}^{3\times3}$ are the observer gain matrices (see Fossen and Strand (1999) for detail). In this bank of observers, we choose small values for $\boldsymbol{K}_3$ to limit the update rate of environmental loads. If there exists a good estimation of $\boldsymbol{b}$, (6c) can be removed. See Hassani and Pascoal (2015) for the assumptions made for development of such model and observer.

3.2 Mooring forces approximation

Due to complexity of the catenary equations, the solution requires iterative techniques. Hence, we use an approximation of the mooring force in the implementation of the observers.

Suppose the heave motion is zero, $z = 0$, there exists a function between the horizontal projected distance X_i and the horizontal restoring component H_i, such that

$$H_i = f_{X_i}(X_i), \quad i = 1, \cdots, M, \tag{7}$$

where $f_{X_i} : D_{X_i} \mapsto \mathbb{R}$ is a locally Lipschitz map from the feasible region $D_{X_i} \subset \mathbb{R}$ into horizontal restoring force. Based on the simulation results, f_{X_i} is continuously strictly monotonic. In this paper, (7) is applied to estimate the restoring force of a single cable.

3.3 Hysteresis switching logic

The switching algorithm is borrowed from Hespanha (2001). The switching logic depends on the estimation errors, defined as

$$\boldsymbol{e}_p := \hat{\boldsymbol{y}}_p - \boldsymbol{y}, \quad p \in \boldsymbol{\mathcal{P}}, \tag{8}$$

where $\hat{\boldsymbol{y}}_p$ is the estimated output of the p^{th} observer. The rational is that under the fault-free condition, e_0 has the smallest norm (in a well defined sense) among the members of the set $\boldsymbol{E} = [e_0, e_1, \cdots, e_M]$. Instead of low-frequency model $\boldsymbol{\eta}_p$, we employ $\hat{\boldsymbol{y}}_p$ here. This is because wave-induced motion does happen to the vessel and is measured

in the GPS signal. When the p^{th} line break occurs, the p^{th} element of $\boldsymbol{\tau}_H$ in (6d) decreases dramatically, and as a consequence $\tilde{\boldsymbol{y}}_p$ changes.

To avoid a chattering problem, a hysteresis-based switching logics is used. The monitoring signals μ_p is then realized by the lowpass filter $\mathbb{G}$, which is given by

$$\dot{\mu}_p = -2\lambda\mu_p + |\boldsymbol{e}_p|_2^2, \quad p \in \boldsymbol{\mathcal{P}}, \tag{9}$$

where $\lambda \in \mathbb{R}$ is a non-negative constant forgetting factor and $|\cdot|_2$ denotes the L_2 norm. Let us define the set $\boldsymbol{\mathcal{N}}$ containing all the monitoring signals, $\mu_p \in \boldsymbol{\mathcal{N}}$.

The present mode of the system (normal condition or line break mode) is determined and identified by the smallest estimation error among all the monitoring signals. The corresponding observer in the bank will perform better in estimating the states of the system; hence, the supervisor detects and isolate the failure, by comparing the performance signals among all the observers. Then the corresponding controller is activated in the feedback loop. The switching signal σ in the feedback loop is determined by the switching logic.

Assume that at the time instant $k-1$, the activated mode is indexed by $\sigma(k-1)$. The scale-independent hysteresis switching logic $\mathbb{S}$ of σ is given by

$$(1+h)\mu_{\sigma(k)} \leq \mu_{\sigma(k-1)}, \tag{10}$$

where $\sigma(k) = \arg\min_p \mu_p(k)$ is the index of the minimum monitoring signal, and $h \in \mathbb{R}$ is a positive constant hysteresis factor. The initial activated mode is the fault-free condition, e.g. $\sigma(0) = 0$. A switching happens at the time instant k, when the minimum member in set $\boldsymbol{\mathcal{N}}$ satisfies (10). The positive constant h here is utilized to delay the switch and reduce the influence from the short-term sensor faults. This switching logic can avoid rapid switches, as well as wear-and-tear effects caused by them. When a switch is triggered, the fault is isolated.

3.4 Controller design

Proposition 3.1. *A PID multi-controller $\mathbb{C}$ is designed based on the certainty equivalence, that is*

$$\boldsymbol{\tau}_c = \boldsymbol{\tau}_{c,pd} + \boldsymbol{\tau}_{c,i}. \tag{11}$$

The PD controller is designed based on backstepping, which is given by

$$\boldsymbol{\tau}_{c,pd} = -\boldsymbol{z}_1 - \boldsymbol{K}_d\boldsymbol{z}_2 + \boldsymbol{D}\boldsymbol{\nu} + \boldsymbol{R}^\top(\psi)\boldsymbol{T}(\boldsymbol{\beta})\hat{\boldsymbol{\tau}}_H + \boldsymbol{M}\dot{\boldsymbol{\alpha}}, \tag{12}$$

where

$$\boldsymbol{\alpha} = -\boldsymbol{K}_p\boldsymbol{z}_1 + \dot{\boldsymbol{\nu}}_d, \tag{13}$$

$$\dot{\boldsymbol{\alpha}} = \boldsymbol{K}_p\boldsymbol{S}(r)\boldsymbol{z}_1 - \boldsymbol{K}_d\boldsymbol{z}_2 + \ddot{\boldsymbol{\nu}}_d, \tag{14}$$

$\boldsymbol{z}_1 = \boldsymbol{R}^\top(\psi)(\hat{\boldsymbol{\eta}} - \boldsymbol{\eta}_d)$, $\boldsymbol{z}_2 = \hat{\boldsymbol{\nu}} - \boldsymbol{\alpha}$, $\boldsymbol{\eta}_d$ is the desired position and heading, $\boldsymbol{\nu}_d$ is the desired velocity generated from the reference system, and $\boldsymbol{S}(r) = -\boldsymbol{S}^\top(r) = \begin{bmatrix} 0 & -r & 0 \\ r & 0 & 0 \\ 0 & 0 & 0 \end{bmatrix}$. $\boldsymbol{K}_p$ and $\boldsymbol{K}_d \in \mathbb{R}^{3\times3}$ are diagonal non-negative PD controller gain matrices. An additional I controller is applied to balance the constant disturbance, which is given by

$$\dot{\boldsymbol{\xi}} = \boldsymbol{\eta} - \boldsymbol{\eta}_d, \tag{15a}$$

$$\boldsymbol{\tau}_{c,i} = -\boldsymbol{K}_i\boldsymbol{R}^\top(\psi)\boldsymbol{\xi}, \tag{15b}$$

where $\boldsymbol{K}_i \in \mathbb{R}^{3\times3}$ is the I controller gain matrix.

Proof. A new bias vector is employed which contains the environmental disturbance and the restoring force caused by mooring line breakage, such that

$$\bar{\boldsymbol{b}}_p := \boldsymbol{b} + \boldsymbol{T}(\boldsymbol{\beta})(\boldsymbol{I} - \boldsymbol{L}_p)\hat{\boldsymbol{\tau}}_H. \tag{16}$$

Substitute (16) into (1) yields the control plant model of P_p,

$$\dot{\boldsymbol{\eta}} = \boldsymbol{R}(\boldsymbol{\psi})\boldsymbol{\nu}, \tag{17a}$$

$$\boldsymbol{M}\dot{\boldsymbol{\nu}} = -\boldsymbol{D}\boldsymbol{\nu} + \boldsymbol{R}^\top(\psi)\boldsymbol{T}(\boldsymbol{\beta})\boldsymbol{\tau}_H + \boldsymbol{\tau}_{\boldsymbol{c}} + \boldsymbol{R}(\psi)^\top\bar{\boldsymbol{b}}_p, \tag{17b}$$

where $\bar{\boldsymbol{b}}_p$ is balanced by the I controller (15). Thereafter, the disturbance is disregarded. Defining the backstepping state transformation

$$\boldsymbol{z}_1 := \boldsymbol{R}^\top(\psi)(\boldsymbol{\eta} - \boldsymbol{\eta}_d) \quad \text{and} \quad \boldsymbol{z}_2 := \boldsymbol{\nu} - \boldsymbol{\alpha}, \tag{18}$$

where η_d is the desired position and heading. Differentiating $\boldsymbol{z}_1$ with respect to time and substitute $\dot{\boldsymbol{R}}(\psi) = \boldsymbol{R}(\psi)\boldsymbol{S}(r)$ into (18), we obtain

$$\dot{\boldsymbol{z}}_1 = -\boldsymbol{S}(r)\boldsymbol{z}_1 + \boldsymbol{z}_2 + \boldsymbol{\alpha} - \boldsymbol{R}^\top(\psi)\dot{\boldsymbol{\eta}}_d. \tag{19}$$

A positive continuous differential Lyapunov function candidate (LFC) is

$$\boldsymbol{V}_1 := \frac{1}{2}\boldsymbol{z}_1^\top\boldsymbol{z}_1, \tag{20}$$

where $\boldsymbol{V}_1$ is positive definite. Due to the property of skew-symmetric matrix, such that $\boldsymbol{z}_1^\top\boldsymbol{S}(r)\boldsymbol{z}_1 = 0$,

$$\dot{\boldsymbol{V}}_1 = \boldsymbol{z}_1^\top(\boldsymbol{\alpha} - \boldsymbol{R}^\top(\psi)\dot{\boldsymbol{\eta}}_d) + \boldsymbol{z}_1^\top\boldsymbol{z}_2. \tag{21}$$

The virtual control is chosen as (13). Substitute (13) into (21), we obtain

$$\dot{\boldsymbol{V}}_1 = -\boldsymbol{z}_1^\top\boldsymbol{K}_p\boldsymbol{z}_1 + \boldsymbol{z}_1^\top\boldsymbol{z}_2 \tag{22}$$

Differentiating $\boldsymbol{z}_2$ with respect to time gives

$$\dot{\boldsymbol{z}}_2 = -\boldsymbol{M}^{-1}\boldsymbol{D}\boldsymbol{\nu} + \boldsymbol{M}^{-1}\boldsymbol{\tau}_c + \boldsymbol{M}^{-1}\boldsymbol{R}^\top(\psi)\boldsymbol{T}(\boldsymbol{\beta})\boldsymbol{\tau}_H - \dot{\boldsymbol{\alpha}}. \tag{23}$$

Choose another LFC as

$$\boldsymbol{V}_2 := \boldsymbol{V}_1 + \frac{1}{2}\boldsymbol{z}_2^\top\boldsymbol{M}\boldsymbol{z}_2. \tag{24}$$

Differentiating the LFC (24) and substituting (23) yield,

$$\begin{aligned}\dot{\boldsymbol{V}}_2 = &-\boldsymbol{z}_1^\top\boldsymbol{K}_p\boldsymbol{z}_1 + \boldsymbol{z}_1^\top\boldsymbol{z}_2 + \boldsymbol{z}_2^\top(-\boldsymbol{D}\boldsymbol{\nu} \\ &- \boldsymbol{R}^\top(\psi)\boldsymbol{T}(\boldsymbol{\beta})\boldsymbol{\tau}_H + \boldsymbol{\tau}_c - \boldsymbol{M}\dot{\boldsymbol{\alpha}}).\end{aligned} \tag{25}$$

Taking the output feedback control law as (12). The differential of the virtual control is (14). The zero dynamics is

$$\dot{\boldsymbol{z}_1} = -(\boldsymbol{S}(r) + \boldsymbol{K}_p)\boldsymbol{z}_1 + \boldsymbol{z}_2, \tag{26a}$$

$$\boldsymbol{M}\dot{\boldsymbol{z}_2} = -\boldsymbol{z}_1 - \boldsymbol{K}_d\boldsymbol{z}_2. \tag{26b}$$

The equilibrium point of the error dynamics $(\boldsymbol{z}_1, \boldsymbol{z}_2) = (\boldsymbol{0}, \boldsymbol{0})$ is uniformly globally asymptotically stable (UGAS). ■

$\boldsymbol{\eta}_d$ and $\boldsymbol{\nu}_d$ can be calculated offline based on setpoint chasing algorithms, such as Nguyen and Sørensen (2009) and Fang et al. (2013).

The control objective of the fault-free mode is to control the heading; therefore, the first two diagonal elements in the control gain matrices are chosen as small values, or simply 0. In these faulty modes, $p \in \boldsymbol{\mathcal{P}}/\{0\}$, the first two diagonal elements in control gain matrices are chosen as larger values to enhance the robustness of the controller (Skjetne and Fossen, 2004).

4 Simulation

4.1 Overview

The simulation is conducted in the MATLAB® and Simulink® environment using the Marine System Simulator (MSS) toolbox from NTNU. The MSS is a Matlab/Simulink library and simulator for marine systems (MSS, 2010). To ensure computational efficiency and save simulation time, a 2D lookup table is used to calculate

the mooring forces from the position of each mooring line terminal point. This 2D lookup table is generated offline iteratively where the inputs are the horizontal distances and the heave motion.

A line break is mainly caused by fatigue, corrosion, or overload. For the sake of simplification, we disregard the situation that another line breaks during the fault detection and isolation period. Hence, this paper focuses on the mooring line failure caused by fatigue and corrosion, after which the vessel can still stay in a safety region. At this moment, the horizontal restoring force provided by the broken line becomes zero. Table 2 presents the main parameters of the simulation model. The ITTC spectrum is used to simulate the irregular waves with a significant wave height $H_s = 5.5\,m$ and mean wave direction $\beta = 45\,deg$. The current is assumed to have a constant speed in the earth frame $v_c = 0.1\,m/s$ and direction $\beta_c = 0\,deg$. The mooring force inputs to the observers are estimated using a 1D lookup table with the collection of the positions and tension data from quasi-static analyses while keeping the heave equal to zero.

Table 2. Vessel main particulars and mooring line dimensions.

Principle Dimension	Values
Dens. of ambient water $\rho_w(kg/m^3)$	1025
Length of the cable $L_m(m)$	2250
Elastic modulus $E_m(Pa)$	4.5757×10^{10}
Cable diameter $d_m(m)$	0.08
Max strain ε	0.005
Position of the anchors (m)	
$[x_{a_1}, y_{a_1}, z_{a_1}]$	$[1950, 0, -1000]$
$[x_{a_2}, y_{a_2}, z_{a_2}]$	$[0, 1950, -1000]$
$[x_{a_3}, y_{a_3}, z_{a_3}]$	$[-1950, 0, -1000]$
$[x_{a_4}, y_{a_4}, z_{a_4}]$	$[0, -1950, -1000]$
$[x_{a_5}, y_{a_5}, z_{a_5}]$	$[1378.9, 1378.9, -1000]$
$[x_{a_6}, y_{a_6}, z_{a_6}]$	$[-1378.9, 1378.9, -1000]$
$[x_{a_7}, y_{a_7}, z_{a_7}]$	$[-1378.9, -1378.9, -1000]$
$[x_{a_8}, y_{a_8}, z_{a_8}]$	$[1378.9, 0, -1000]$

The FPSO is initially moored by all eight mooring lines in Fig. 1. In this simulation, line breakage happens at $t_f = 250$ seconds in 1) Line 3 (P_3); 2) Line 7 (P_7); and 3) Line 8 (P_8).

4.2 Results and discussion

Fig. 4 to Fig. 6 present the results.

1) Fig. 4 is the simulation result when Line 3 breaks. The correct controller is activated about 30 seconds after line break. The decrease rate of the monitoring signal from failure line is faster than any other signals.

2) Fig. 5 shows the responses when Line 7 breaks. The fault diagnosis is slower with a faulty isolated mode at the first 70 seconds after the break. Monitoring signal from Line 3 decreases faster at the beginning 40 seconds, so for short amount of time a wrong model (break of line 3) is selected. However, soon after the right line break model is identified.

3) Fig. 6 shows the result when Line 8 breaks. The supervisor can activate the faulty mode within 20 seconds. The monitoring signals from other lines except Line 8 are all much larger than the signal from Line 7.

5 Conclusion and Future Work

This paper presented a fault-tolerant control scheme based on an estimator-based supervisory control methodology. An online fault diagnosis algorithm was designed based on residual signals from a pre-designed bank of observers. The simulation conducted for a moored FPSO demonstrated effectiveness of the proposed tool.

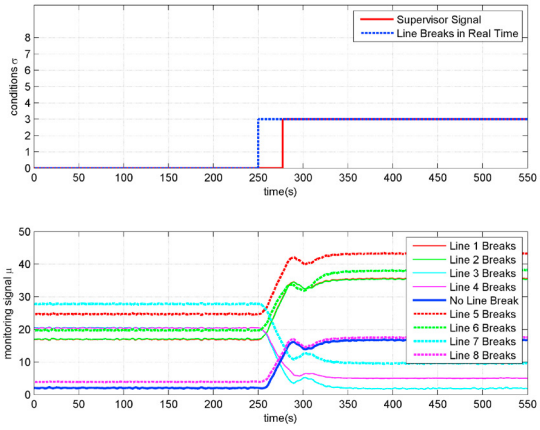

Fig. 4. Evolution of switching signal and monitoring signals during the Simulation. Line 3 breaks at 250s.

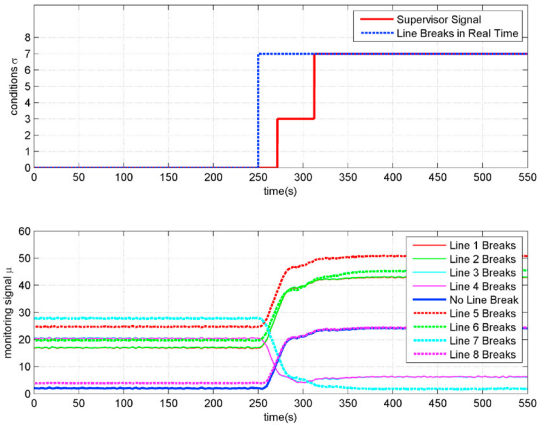

Fig. 5. Evolution of switching signal and monitoring signals during the Simulation. Line 7 breaks at 250s.

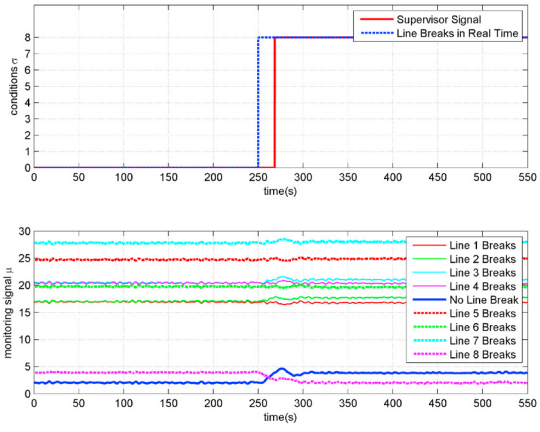

Fig. 6. Evolution of switching signal and monitoring signals during the Simulation. Line 8 breaks at 250s.

Future work will include the application of the methodology developed to a higher fidelity model of moored vessels. The effects of environmental loads on the detection performance will be further studied, as well as a quantification of false alarms and unsuccessful detections.

Acknowledgements

This work was supported by the Research Council of Norway (RCN) through the Centre for Research-based Innovation on Marine Operations (CRI MOVE), and the Centre of Excellence AMOS (RCN-project 223254). We thank Prof. Mogens Blanke for many discussions on fault tolerant control. We would also like to thank Hans-Martin Heyn for his assistance during the the preparations of this article.

References

Aamo, O.M. and Fossen, T.I. (1999). Controlling line tension in thruster assisted mooring systems. In *Control Applications, 1999. Proceedings of the 1999 IEEE International Conference on*, volume 2, 1104–1109 vol. 2.

Aamo, O.M. and Fossen, T.I. (2001). Finite element modelling of moored vessels. *Mathematical and Computer Modelling of Dynamical Systems*, 7(1), 47–75.

ABS (2014). Guide for building and classing mobile offshore units.

API, R. (2005). 2sk (2005) design and analysis of stationkeeping systems for floating structures.

Balchen, J.G., Jenssen, N.A., Mathisen, E., and Sælid, S. (1980). A dynamic positioning system based on kalman filtering and optimal control. *Modeling, Identification and Control (MIC)*, 1, 135–163.

Balchen, J.G., Jenssen, N.A., and Sælid, S. (1976). Dynamic positioning using kalman filtering and optimal control theory. In *IFAC/IFIP symposium on automation in offshore oil field operation*, volume 183, 183–186.

Berntsen, P.I.B., Aamo, O.M., and Leira, B.J. (2009). Ensuring mooring line integrity by dynamic positioning: Controller design and experimental tests. *Automatica*, 45(5), 1285–1290.

Berntsen, P.I.B., Aamo, O.M., Leira, B.J., and Ieee (2006). Dynamic positioning of moored vessels based on structural reliability. In *Proceedings of the 45th Ieee Conference on Decision and Control, Vols 1-14*, IEEE Conference on Decision and Control, 5906–5911. doi: 10.1109/cdc.2006.377085.

Brown, M.G., Hall, T.D., Marr, D.G., English, M., and Snell, R.O. (2005). Floating production mooring integrity jip - key findings. doi:10.4043/17499-MS.

Chen, M., Ge, S.S., How, B.V.E., and Choo, Y.S. (2013). Robust adaptive position mooring control for marine vessels. *Ieee Transactions on Control Systems Technology*, 21(2), 395–409.

DNV (2010). Dnv-os-e301: Offshore standard-position mooring.

Elman, P., Elletson, E., and Bramande, J. (2013). Reducing uncertainty through the use of mooring line monitoring. In *Offshore Technology Conference*, 29–31. Rio de Janeiro, Brazi.

Fang, S. and Blanke, M. (2011). Fault monitoring and fault recovery control for position-moored vessels. *International Journal of Applied Mathematics and Computer Science*, 21(3), 467–478.

Fang, S., Blanke, M., and Leira, B.J. (2015). Mooring system diagnosis and structural reliability control for position moored vessels. *Control engineering Practice*, 36, 12–26.

Fang, S., Leira, B.J., and Blanke, M. (2013). Position mooring control based on a structural reliability criterion. *Structural Safety*, 41, 97–106.

Fossen, T.I. and Grøvlen, A. (1998). Nonlinear output feedback control of dynamically positioned ships using vectorial observer backstepping. *Control Systems Technology, IEEE Transactions on*, 6(1), 121–128.

Fossen, T.I. (2011). *Handbook of marine craft hydrodynamics and motion control*. John Wiley & Sons.

Fossen, T.I. and Strand, J.P. (1999). Passive nonlinear observer design for ships using lyapunov methods: full-scale experiments with a supply vessel. *Automatica*, 35(1), 3–16.

Gauthier, S., Elletson, E., et al. (2014). Mooring line monitoring to reduce risk of line failure. In *The Twenty-fourth International Ocean and Polar Engineering Conference*. International Society of Offshore and Polar Engineers.

Hassani, V. and Pascoal, A. (2015). Wave filtering and dynamic positioning of marine vessels using a linear design model: Theory and experiments. In C. Ocampo-Martinez and R.R. Negenborn (eds.), *Transport of Water versus Transport over Water*, volume 58 of *Operations Research/Computer Science Interfaces Series*, 315–343. Springer International Publishing.

Hassani, V., Sørensen, A., and Pascoal, A.M. (2012a). Robust dynamic positioning of offshore vessels using mixed-μ synthesis, Part I: A control system design methodology. In *1st IFAC Workshop on Automatic Control of Offshore Oil and Gas Production*. Trondheim Norway.

Hassani, V., Sørensen, A.J., and Pascoal, A.M. (2012b). Robust dynamic positioning of offshore vessels using mixed-μ synthesis, Part II: Simulation and experimental results. In *1st IFAC Workshop on Automatic Control of Offshore Oil and Gas Production*. Trondheim Norway.

Hespanha, J.P. (2001). Tutorial on supervisory control. In *Lecture Notes for the workshop Control using Logic and Switching for the 40th Conf. on Decision and Contr., Orlando, Florida*.

MSS. Marine Systems Simulator (2010). Viewed 30.10.2014. URL `http://www.marinecontrol.org`.

Nguyen, D.H., Nguyen, D.T., Quek, S.T., and Sørensen, A.J. (2011). Position-moored drilling vessel in level ice by control of riser end angles. *Cold Regions Science and Technology*, 66(2-3), 65–74.

Nguyen, D.T. and Sørensen, A.J. (2009). Setpoint chasing for thruster-assisted position mooring. *Ieee Journal of Oceanic Engineering*, 34(4), 548–558.

Nguyen, T.D., Sørensen, A.J., and Tong Quek, S. (2007). Design of hybrid controller for dynamic positioning from calm to extreme sea conditions. *Automatica*, 43(5), 768–785.

Skjetne, R. and Fossen, T.I. (2004). On integral control in backstepping: analysis of different techniques. 2.

Stoican, F. and Olaru, S. (2013). *Set-theoretic Fault-tolerant Control in Multisensor Systems*. John Wiley & Sons.

Tannuri, E.A., Donha, D.C., and Pesce, C.P. (2001). Dynamic positioning of a turret moored FPSO using sliding mode control. *International Journal of Robust and Nonlinear Control*, 11(13), 1239–1256. doi:10.1002/rnc.604.